VIP Biocatalysis Very Important Paper

How to cite: *Angew. Chem. Int. Ed.* **2021**, *60*, 5913–5920
International Edition: doi.org/10.1002/anie.202014771
German Edition: doi.org/10.1002/ange.202014771

In Vivo Assembly of Artificial Metalloenzymes and Application in Whole-Cell Biocatalysis**

*Shreyans Chordia, Siddarth Narasimhan, Alessandra Lucini Paioni, Marc Baldus, and Gerard Roelfes**

Abstract: *We report the supramolecular assembly of artificial metalloenzymes (ArMs), based on the Lactococcal multidrug resistance regulator (LmrR) and an exogeneous copper(II)–phenanthroline complex, in the cytoplasm of E. coli cells. A combination of catalysis, cell-fractionation, and inhibitor experiments, supplemented with in-cell solid-state NMR spectroscopy, confirmed the in-cell assembly. The ArM-containing whole cells were active in the catalysis of the enantioselective Friedel–Crafts alkylation of indoles and the Diels–Alder reaction of azachalcone with cyclopentadiene. Directed evolution resulted in two different improved mutants for both reactions, LmrR_A92E_M8D and LmrR_A92E_V15A, respectively. The whole-cell ArM system required no engineering of the microbial host, the protein scaffold, or the cofactor to achieve ArM assembly and catalysis. We consider this a key step towards integrating abiological catalysis with biosynthesis to generate a hybrid metabolism.*

Introduction

Artificial metalloenzymes (ArM), which are hybrids of catalytically active transition metal complexes embedded in protein scaffolds, have emerged as a promising approach for biocatalysis of reactions that have no equivalent in nature.[1,2] This approach gives rise to rudimentary enzymes that can subsequently be tailored for the reaction of interest by employing the power of site-directed mutagenesis and/or directed evolution.[3–5] For further developments, it is highly desirable to achieve the assembly and application of ArMs in bacterial cells. This will allow for whole cell biocatalysis, which is attractive from an economical perspective, is convenient for directed evolution and ultimately will be important towards achieving the goal of creating a hybrid metabolism, that is, a biosynthetic pathway augmented with new-to-nature chemistry.[6] Yet, application in whole cells present some major challenges, which include assembly of the artificial enzyme from a heterologously expressed protein and an exogenously added metal complex and the mutual incompatibility and inactivation of transition metal complexes and biological components, in particular glutathione.[7–9] Recently, the first reports of application of ArMs in cells appeared. In these studies, the above-mentioned challenges were circumvented by creating the ArM in the periplasm or on the cell surface, where the GSH concentration is minimal and there are less barriers to achieving incorporation of the metal cofactor.[10–15] Cytoplasmic assembly has been achieved for artificial metallo-heme enzymes, using bacteria containing co-expressed natural and engineered heme transporters.[16–19]

Previously, we have reported on ArMs based on the Lactococcal multidrug resistance regulator (LmrR) protein from Lactococcus lactis.[20] LmrR is a transcription factor that forms a homodimer with a large hydrophobic pocket, known to promiscuously bind many small planar compounds.[21] We have shown that ArMs can be formed from LmrR by self-assembly upon addition of a copper(II) 1,10-phenanthroline complex (Cu^{II}-Phen).[22,23] The Cu^{II}-Phen complex binds to LmrR with low micromolar affinity and is primarily located between the two central tryptophans, one from each monomer (W96/W96′). This ArM was found to be an excellent catalyst for the enantioselective vinylogous Friedel–Crafts alkylation of indoles. Moreover, mutagenesis of residues in the hydrophobic pocket showed significant effect on catalysis, with a few mutations, notably M8A and A92E giving rise to significant improvement of activity and selectivity of the catalyzed reaction.[24]

Herein, we report the spontaneous self-assembly of functional LmrR-based ArMs in the cytoplasm of *Escherichia coli* and subsequent application in whole cell biocatalysis and directed evolution.

[*] S. Chordia, Prof. Dr. G. Roelfes
Stratingh Institute for Chemistry, University of Groningen
Nijenborgh 4, 9747 AG Groningen (The Netherlands)
E-mail: j.g.roelfes@rug.nl
Dr. S. Narasimhan, Dr. A. Lucini Paioni, Prof. Dr. M. Baldus
NMR Spectroscopy group, Bijvoet Center for Biomolecular Research
Utrecht University
Padualaan 8, 3584 CH Utrecht (The Netherlands)
Dr. S. Narasimhan
Current address: Structural and Computational Biology Unit
European Molecular Biology Laboratory
Meyerhofstraße 1, 69117 Heidelberg (Germany)

[**] A previous version of this manuscript has been deposited on a preprint server (https://doi.org/10.26434/chemrxiv.12485993.v1).

Supporting information and the ORCID identification number(s) for the author(s) of this article can be found under: https://doi.org/10.1002/anie.202014771.

Results and Discussion

Catalysis in Whole Cells

To establish the tolerance of LmrR/Cu^{II}-Phen against cellular components, we performed the catalysis of the reaction of α,β-unsaturated 2-acyl-1-methylimidazole (**1**) with 2-methylindole (**2a**) in cell-free extracts. For this purpose, LmrR was expressed heterologously in *E. coli* C43(DE3) cells, the cells were lysed and the cell debris pelleted to yield cell free extracts, to which Cu^{II}-Phen was added. Significant catalysis and enantioselective product formation was observed (Figure 1b). In contrast, expressing Small Ubiquitin-like MOdifier (SUMO) as a control protein in combination with Cu^{II}-Phen only gave rise to low yield of product and low enantioselectivity in cell-free extract.

Next, we took the whole *E. coli* cells expressing LmrR and incubated them with Cu^{II}-Phen. The cells were then washed to remove excess, unbound Cu^{II}-Phen and incubated with substrates (Figure 1a). Remarkably, we still observed accelerated catalysis and enantioselective product formation. In the absence of Cu^{II}-Phen, or using SUMO instead of LmrR did not give rise to catalysis. Thus, it was confirmed that both LmrR protein and exogenously added Cu^{II}-Phen are essential for catalysis.

To confirm that the catalysis occurs in the cells, we incubated *E. coli* cells expressing LmrR with Cu^{II}-Phen for 1 h and then pelleted the cells and washed with buffer to remove unbound Cu^{II}-Phen. The copper content of the cells was quantified using inductively coupled plasma optical emission spectrometry (ICP-OES; Figure 1c). The data shows that a significant portion of the copper added is retained by the cell fraction suggesting the cells did indeed take up the Cu^{II}-Phen complex. Comparison of the relative amounts of copper found in the cell fraction and supernatant fraction suggest that the overall concentration of Cu^{II}-Phen in the cell fraction sample is around 50 μM. Notably, this does not necessarily mean that all this Cu^{II}-Phen has been internalized; it also includes the possibility of copper complex that is bound on the surface of the cells. Based on the protein expression yields, the overall concentration of LmrR in the sample is in the low μM range and, hence, the Cu^{II}-Phen is present in excess. It should be noted that the local concentration of the ArM in the cells will be significantly higher. The excess Cu^{II}-Phen will contribute to the background reaction, causing a lowering of the *ee* value as compared to the experiments with isolated protein. Yet, the control experiments with SUMO (Figure 1a) and the combined enantioselective catalysis results (vide infra) show that the overall

a

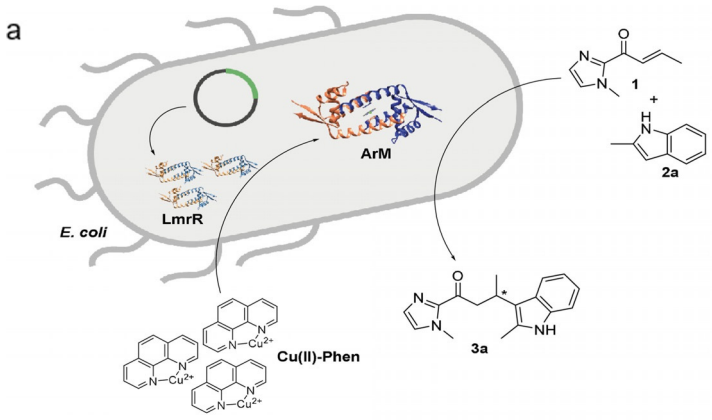

b

	Yield (%)	ee (%)
Cell free extract:		
LmrR/Cu(II)-Phen	22±3	72±4
SUMO/Cu(II)-Phen	11±2	13±8
Whole cells:		
LmrR	0	-
LmrR/Cu(II)-Phen	24±6	69±13
SUMO/Cu(II)-Phen	11±6	<5

c

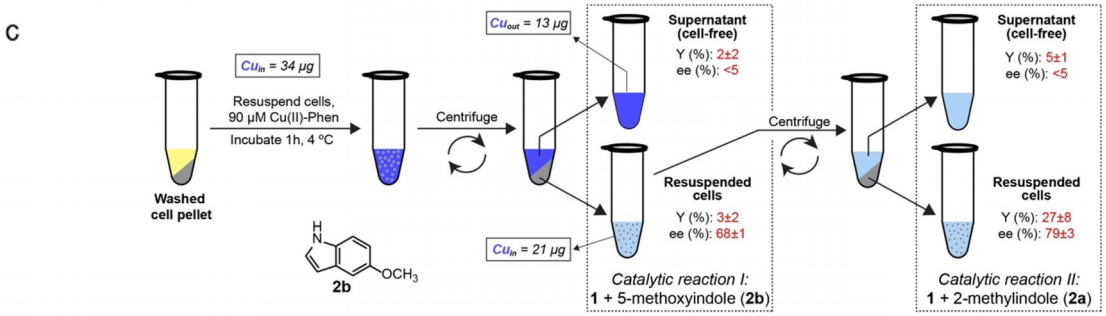

Figure 1. a) Self-assembly of Cu^{II}-Phen/LmrR artificial metalloenzyme in *E. coli* cells and catalyzed enantioselective Friedel–Crafts alkylation reaction. b) Results of catalysis of the enantioselective Friedel–Crafts alkylation reaction of **1** with **2a** by Cu^{II}-Phen/LmrR and Cu^{II}-Phen/SUMO in cell-free extract and whole cells. In vitro catalysis: 120 μM LmrR, 90 μM Cu^{II}-Phen, 1 mM **1** and **2a** in 20 mM MOPS, 150 mM NaCl, pH 7 at 4 °C for 30 min; in vivo catalysis: *E. coli* C43(DE3) cells over-expressing LmrR (from a 0.5 mL overnight culture; $OD_{600nm} = 4$), 90 μM Cu^{II}-Phen, 1 mM **1** and **2a** in catalysis buffer at 4 °C. Values are given as the average of independent duplicate experiments, each performed in duplo. Errors margins are standard deviations. c) Experimental design of the catalysis experiments with whole cells and supernatant. Values of copper content as determined by ICP-OES are given in solid boxes. In dashed boxes are the samples that were used for catalytic reaction I: the Friedel–Crafts alkylation of **2b** with **1**, and catalytic reaction II: the Friedel–Crafts alkylation of **2a** with **1**.

outcome of catalysis is dominated by the ArM, due to the rate acceleration it provides.

The cell and the supernatant fractions were both incubated with substrates **1** and **2b** for the Friedel–Crafts alkylation reaction. Low activity was observed in both cases, which is in part related to the fact that **2b** is a less preferred substrate for LmrR/Cu^{II}-Phen (see below), but only in the cell fraction significant enantioselectivity was observed in the product (Figure 1b). The cell fraction was then again subjected to the same procedure and then a fresh batch of substrates, in this case **1** and **2a**, which is a preferred indole,[22] was added. Again, enantioselective product formation was only observed from the cell sample. These results confirm that the ArM assembled in the cell is responsible for this catalysis. Moreover, it also shows that the ArM has not leaked out into the buffer/supernatant, indicating that the structural integrity of cells is preserved.

Next, a series of LmrR mutants, for which the activity and enantioselectivity is known were tested in the cell experiments.[24] A good correlation was observed between activity and selectivity of the isolated ArM and that of the ArM in whole cells, even though the enantioselectivities in whole cells were generally lower than those found with isolated enzymes, most likely due to the background reaction (Figure 2a, Table S1). For example, the mutant A92E, which we reported as the most active and selective ArM to date for this reaction[24] also gives significantly higher yield and enantioselectivity than the wild type in the cell experiments. Similarly, mutations that had a detrimental effect on catalysis in isolated proteins also showed this effect in cells.

From previous work on the LmrR protein we know that it binds Hoechst 33342 and ethidium bromide with high affinity in its hydrophobic pocket and that they can inhibit catalysis by competing for binding with Cu^{II}-Phen and the substrates.[24] Hoechst 33342 is cell permeable, whereas ethidium has

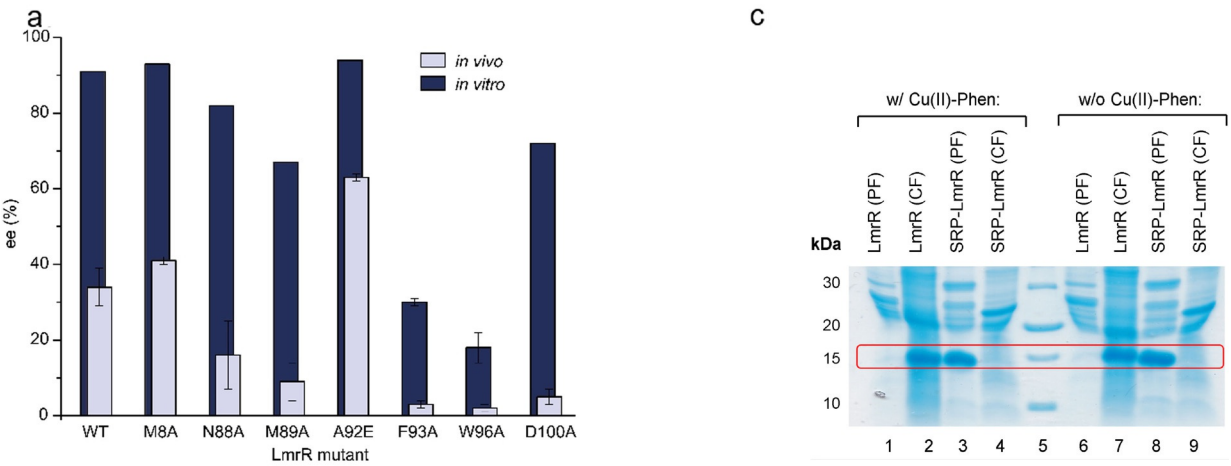

b

	Yield (%)	ee (%)
in vitro:		
no inhibitor	60±2	90±1
Hoechst 33342	12±3	40±1
EtBr	9±3	70±0
in vivo:		
no inhibitor	18±1	77±1
Hoechst 33342	10±1	26±3
EtBr	15±3	71±0

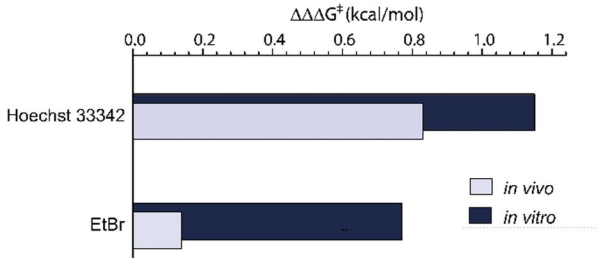

Figure 2. a) Enantioselectivity of the Friedel–Crafts alkylation reaction of **1** with **2a**, catalyzed by isolated Cu^{II}-Phen/LmrR artificial enzyme mutants (dark blue) and Cu^{II}-Phen/LmrR artificial enzyme mutants in whole *E. coli* cells (light blue). b) Left: Effect of addition of Hoechst 33342 and ethidium bromide (EtBr; 4 equivalents compared to Cu^{II}-phen) on the yield and enantioselectivity of the reaction of **1** with **2b**, catalyzed by isolated Cu^{II}-Phen/LmrR artificial metalloenyzmes and in whole cells. Values are given as the average of independent duplicate experiments, each performed in duplo. Errors are given as standard deviations. Right: Difference in enantioselectivity in the reaction of **1** with **2b** catalyzed by isolated Cu^{II}-Phen/LmrR artificial metalloenzymes (dark blue bars) and in whole cells (light blue bars upon addition of inhibitors, compared to w/o inhibitor). A larger bar signifies a larger effect of the inhibitor on the enantioselectivity. Enantioselectivity differences are represented as $\Delta\Delta\Delta G^{\ddagger}$, which is calculated using $\Delta\Delta\Delta G^{\ddagger} = \Delta\Delta G^{\ddagger}_{(\text{w/o inhibitor})} - \Delta\Delta G^{\ddagger}_{(\text{w inhibitor})}$ and $\Delta\Delta G^{\ddagger} = RT\ln(er)$, in which er is the enantiomeric ratio: % major enantiomer/% minor enantiomer. c) SDS PAGE of a *E. coli* cell fractionation experiment to determine protein localization for LmrR and SRP-LmrR with and without Cu^{II}-Phen. PF = periplasmic fraction; CF = cytoplasmic fraction.

difficulties crossing the double membrane barrier of *E. coli* and is normally used to stain dead *E. coli* cells, which have permeable cell membranes. Fluorescence microscopy confirmed that Hoechst 33342 was readily taken up by the LmrR expressing cells, whereas ethidium bromide was not (Figures S4–S6). Indeed, using these dyes in combination with isolated LmrR/Cu^{II}-Phen gave rise to a strongly reduced yield and enantioselectivity in catalysis in the reaction of **1** with **2b** (Figure 2b). Incubating *E. coli* cells expressing LmrR with Hoechst 33342 prior to addition of Cu^{II}-Phen, we found that in catalysis the enantioselectivity of the product was significantly decreased. In contrast, no significant effect on the enantioselectivity was observed for cells incubated with ethidium bromide. This becomes especially apparent when expressing the enantioselectivity differences w/ and w/o inhibitor in $\Delta\Delta\Delta G^{\ddagger}$ (Figure 2b, inset).

We further investigated the cellular localization of Cu^{II}-Phen/LmrR in *E. coli* by performing cell fractionation experiments. These experiments showed that LmrR and Cu^{II}-Phen/LmrR are localized exclusively in the cytoplasm of *E. coli* (Figure 2c). This strongly suggests that the ArM assembles in the cytoplasm of *E. coli.* For comparison, a variant of LmrR (called SRP-LmrR) containing a N-terminal periplasmic localization signal known to transport proteins to the periplasm through the SRP pathway, was constructed.[25] As expected, SRP-LmrR and Cu^{II}-Phen/SRP-LmrR were found to exclusively localize in the periplasm of *E. coli.*

Combined these experiments support that the LmrR/Cu^{II}-Phen ArM is assembled in the cytoplasm of *E. coli* and that the structural integrity of the cellular membrane is maintained during the experiments.

In-Cell NMR Studies of ArM Assembly

While the reactivity data is fully in agreement with in vivo assembly of the ArM, it does not provide direct evidence. For this reason, the assembly of the ArM in *E. coli* Lemo21 (DE3) cells was studied by in-cell NMR spectroscopy. We focused on the LmrR_A92E mutant, since this has a higher binding affinity for Cu^{II}-Phen.[24] Due to high molecular crowding in *E. coli* cells,[26] in-cell solution-state NMR spectroscopy was not feasible.[27] Instead, we employed dynamic nuclear polarization (DNP)-supported solid-state NMR (DNP-ssNMR) spectroscopy, which can probe protein structure inside cells irrespective of protein size and molecular crowding at greatly enhanced sensitivity.[28,29] For reference, we first obtained solution- and solid-state NMR evidence for in vitro assembly of the ArM using near-complete resonance assignments (Figure 3a, see also Tables S9, S10) and by probing paramagnetic quenching effects exerted by Cu^{II}. 2D experiments in both soluble (Figures S10, S11) and microcrystalline (Figure S12) samples revealed site-selective paramagnetic quenching, along with faster longitudinal relaxation rates (R1) in the ssNMR spectra (Figure S13). Additionally, small chemical shift perturbations (CSPs) occurred in the residues away from the Cu^{II}-Phen binding site (Figure S14), consistent with the structural plasticity exhibited by LmrR when bound to different compounds.[21,30–32]

For the in-cell DNP-ssNMR experiments, LmrR-specific isotope labeling was achieved using the antibiotic rifampicin to suppress native *E. coli* polymerases during T7 RNA polymerase mediated expression.[33–36] The signal contributions from the cellular background were reduced further by eliminating the non-protein cellular background labeling using a specialized algal amino-acid mixture (devoid of Trp, Cys, Asn and Gln) for isotope labeling.[37] Secondly, the cellular background was deuterated, which also leads to high DNP enhancements on the molecule of interest.[38] Lastly signal contributions from unincorporated, isotope labeled amino acids were removed by expressing in unlabeled medium during the last quarter of the expression time. The resulting in-cell DNP-ssNMR samples exhibited an approximately 100-fold increase in LmrR signals (Figure S15a) and allowed us to rapidly record different multidimensional ssNMR experiments. The 2D DNP-ssNMR spectra (Figure S16, S17) were in very good agreement with the in vitro spectrum of LmrR. In line with our 2D data sets, analysis of the 3D data sets suggested qualitative agreement between our in vitro assignments and the backbone correlations observed in cells. In spite of the increased NMR line width at low-temperature 400 MHz DNP conditions,[39] we could obtain several spectral strips in the 3D experiment (see materials and methods) which unambiguously matched with the backbone assignments determined in vitro (Figure 3b, Figures S18–S20). We correlated the Cα, Cβ assignments to the side chains and the carbonyl chemical shifts to confirm the respective amino acid type (Figure 3b). The solution-state NMR spectrum of the lysates further confirmed that well folded LmrR is the only labeled molecule in the sample, and additionally showed no visible signs of protein degradation (Figure S21).

As a final test for assembly of the ArM in cells, we tracked the paramagnetic effect of adding Cu^{II}-Phen upon Trp NMR resonances of LmrR. For this purpose, a modified expression protocol was used (SI Material and Methods NMR studies) that led to the labeling of all amino acids, including Trp. In the presence of Cu^{II}-Phen, we observed a selective reduction of the Trp aromatic side-chain signal intensity, while Tyr residues, which are present far away from the Cu^{II}-Phen binding region, do not display paramagnetic quenching effects (Figure 3a,c and Figure S22). Additionally, a clear increase in the longitudinal relaxation rate (R1) was also observed (Figure S23) in full accordance with the spectral changes observed in vitro (Figure 3c, Figure S12, S13). To validate our DNP-ssNMR analysis, we finally analyzed the clear cell lysates of replicate cells used for in vivo DNP-ssNMR experiments using solution NMR (Figure S24). The CSPs due to Cu^{II}-Phen binding largely followed a similar trend to in vitro CSPs (Figure S25), and we observed a complete quenching of Trp96 side chain resonance (Figure S24, S26) suggesting tight binding to the protein, indicating the presence of stably assembled ArM in the lysate.

Taken together, these results provide direct spectroscopic evidence for the in vivo assembly of the ArM. Moreover, the copper complex is predominantly present in the Cu^{II} state. This is consistent with the observed activity in catalysis, further confirming that the reduction of Cu^{II} to Cu^{I},[40] due to cellular reductants, does not play a significant role.

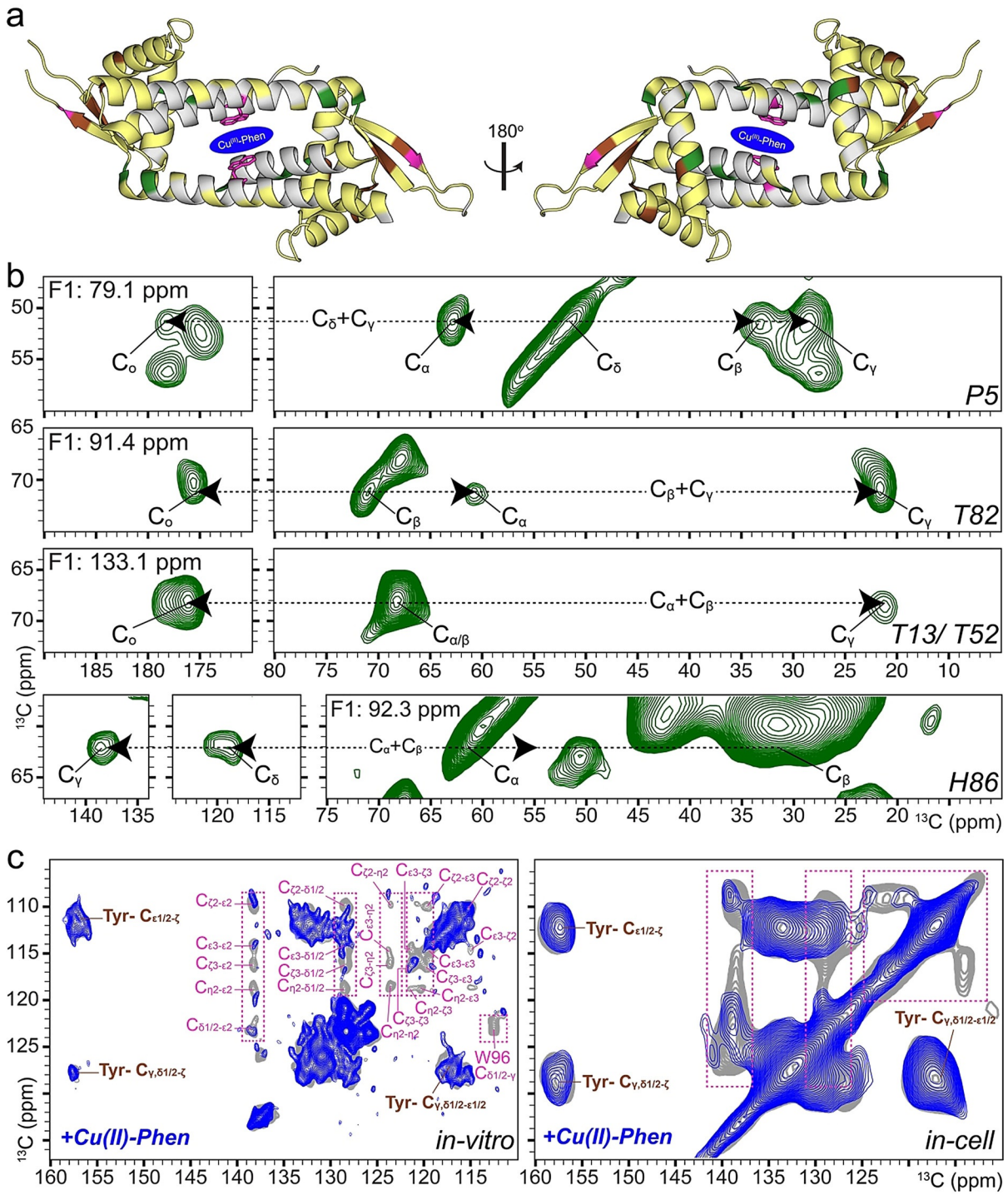

Figure 3. In vitro and in-cell NMR studies of the LmrR_A92E/Cu^{II}-Phen artificial metalloenzyme. a) Summary of NMR analysis: Residues used for both solution- and solid-state NMR analysis are plotted on the crystal structure of LmrR (PDB ID: 3F8F) in yellow, green, pink and brown. Green residues were identified in the 3D ^{13}C (DQ-SQ-SQ) DNP-ssNMR spectrum (b). Tryptophan (pink) and tyrosine (brown) residues are used for analysis in (c), in which the selective reduction of NMR signal intensities for Trp aromatic signals confirms proper in-cell assembly of the ArM. In-cell experiments were performed in *E. coli* Lemo21 (DE3).

Directed Evolution

Having established that these LmrR based ArMs are assembled in vivo and can be employed in whole cell biocatalysis, we aimed to exploit this for directed evolution of the ArMs. The reaction of enone 1 with 5-methoxyindole (**2b**), which is a less good substrate than 2-methylindole (**2a**) for enantioselective vinylogous Friedel–Crafts alkylation, was selected for this purpose. An Alanine scan of residues in the hydrophobic pocket of LmrR was performed to identify

positions of interest (Table S2). The trend of enantioselectivity from in vivo catalysis and activity from in vitro catalysis matched well for the Alanine mutants (Figure 2a).

LmrR_A92E was chosen as the starting point for directed evolution because it was shown to be significantly more active than LmrR.[24] Site-saturation libraries with NDT codon degeneracy were designed for positions 8, 14, 88, 89, 93 and 100, which were identified in the alanine scan as positions of interest (Figure 4a). From one round of screening (in total ca. 250 clones) the mutant LmR_A92E_M8D was found to show the highest activity and enantioselectivity (Table S14). Enzyme kinetics studies for the reaction of **1** and **2b** confirmed that the catalytic efficiency (k_{cat}/K_M) of LmrR_A92E_M8D was 185.9 $M^{-1}min^{-1}$, almost three times higher than that of the starting point, LmrR_A92E (73.3 $M^{-1}min^{-1}$; Figure S29). While M8 in LmrR was known from previous studies to be a privileged residue for ArM optimization,[24,41,42] this always entailed mutation to another hydrophobic residue and the mutation M8D was not found before as beneficial for catalysis.

The scope of indoles was compared for ArMs based on three LmrR variants: LmrR, LmrR_A92E and LmrR_A92E_M8D) (Figure 4b). A marked improvement in activity from LmrR to LmrR_A92E for the different indoles was found. This was further improved for the double mutant LmrR_A92E_M8D for all the indoles tested. It is remarkable to see that almost 40% of **2a** is converted to product in thirty minutes by LmrR_A92E_M8D. This demonstrates that directed evolution is a powerful tool for improving the catalytic properties of ArM.

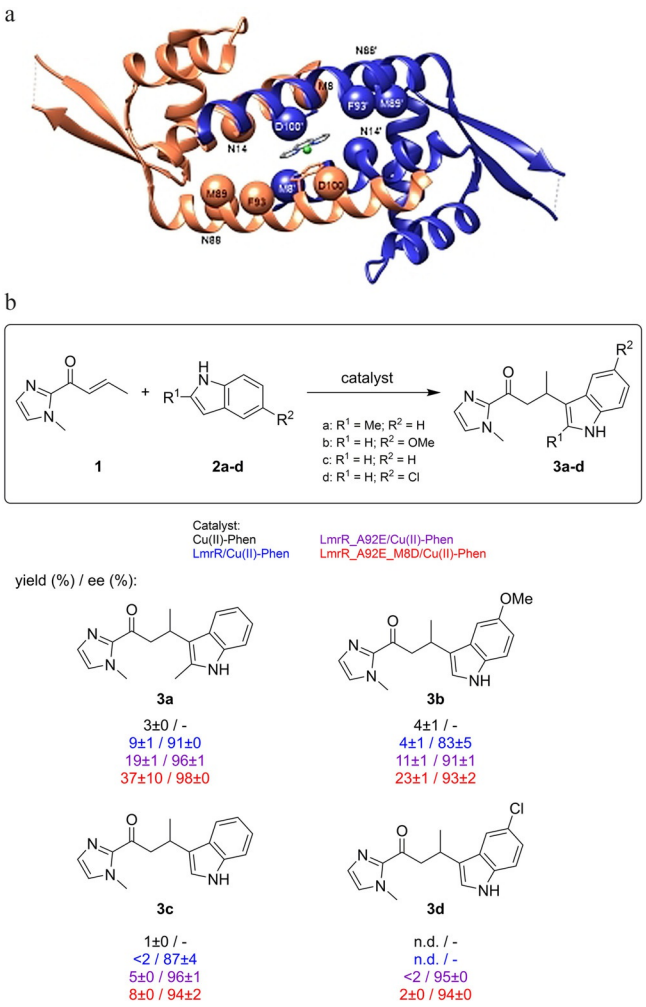

Figure 4. a) Structure of LmrR/Cu^{II}-Phen with residues that were randomized during the directed evolution study indicated as spheres. b) Scope of the enantioselective Friedel–Crafts alkylation catalyzed by Cu^{II}-Phen and Cu^{II}-Phen/LmrR artificial metalloenzyme mutants. Conditions: 12 μM LmrR mutant, 9 μM Cu^{II}-Phen, 1 mM **1** and **2a** in 20 mM MOPS, 150 mM NaCl, pH 7 at 4 °C. Reaction times: 30 min (**3a**), 6 h (**3b**, **3c**) or 24 h (**3d**). Values are given as the average of independent duplicate experiments, each performed in duplo. Errors are given as standard deviations.

In Vivo ArM Catalysis of Diels–Alder Reactions

Having established the in vivo ArM-catalyzed Friedel–Crafts alkylation, we sought to expand the scope to a different catalytic reaction. For this purpose, we selected the Cu^{II} catalyzed Diels–Alder reaction of azachalcone (**4**) with cyclopentadiene (**5**) (Table 1).[43] This is a reaction that we have reported on before using ArMs based on LmrR with covalently attached phenanthroline and bipyridine ligands,[44] but it was so far not investigated with supramolecular assembled ArMs. Performing the reaction with isolated wtLmrR/Cu^{II}-Phen after 2 days of reaction provided the *endo* isomer of the Diels–Alder product **6** with 58% *ee* (Table 1). Using whole cells containing the ArMs, assembled as described above, the Diels–Alder product was obtained in about 14% yield with 8% *ee* after 3 days, whereas control experiments with SUMO instead of LmrR resulted in racemic product. LmrR_A92E gave rise to a higher *ee* value, both in vitro and in vivo, confirming that also for this reaction the effect of mutations is detectable in the whole cell experiments (Table 1). Therefore, an alanine scan of various positions in

Table 1: Results of the in vivo and in vitro ArM-catalyzed Diels–Alder reaction.

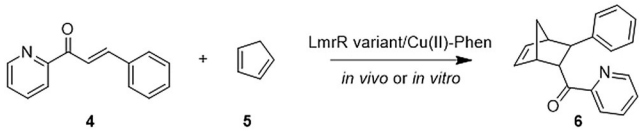

Protein	In vivo[a]		In vitro[b]	
	yield [%][c]	*ee* [%][c]	yield [%][c]	*ee* [%][c]
SUMO	14±1	0		
LmrR	14±4	8±2	22±5	58±6
LmrR_A92E	15±6	17±1	33±10	68±2
LmrR_A92E_V15A	20±3	45±0	52±7	84±3

[a] Cu^{II}-Phen (180 μM), *E. coli* cell suspension (1 mL), **4** (1 mM) and **5** (33 mM) in 20 mM MOPS, 150 mM NaCl at pH 7, reaction time 48 h at 4 °C. [b] Cu^{II}-Phen (90 μM), LmrR variant (120 μM), **4** (1 mM) and **5** (33 mM) in 20 mM MOPS, 150 mM NaCl at pH 7, reaction time 48 h at 4 °C. [c] Values for the *endo* isomer. Values represent the average of independent duplicate experiments, each performed in duplo. Errors are given as standard deviations.

LmrR and LmrR_A92E was performed to identify residues that could potentially be mutated to improve the ArM. Whole cell experiments with the various mutant ArMs showed detectable differences in both yield and enantioselectivity (Table S5). The results were verified independently with isolated ArMs and, even though the yields and *ee* values in the whole cell catalysis experiments were generally lower, a good correlation of the trends in yields and *ee* values was observed. From the whole cell experiments one variant, LmrR_A92E_V15A, was identified that gave rise to both higher yield and *ee*, that is, 20 and 45%, respectively. This was confirmed in vitro using the isolated protein, giving the Diels–Alder product in 52% yield and 84% *ee* (Table 1). Control experiments with this mutant confirmed that the catalysis indeed occurred inside cells (Table S6).

Attempted directed evolution by randomization of 7 positions that were deemed potentially interesting from the alanine scanning did not result in further improved variants. Nevertheless, LmrR_A92E_V15A is a new variant: it was not found before as improved mutant in other reactions. Interestingly, this mutant performed poorly in the Friedel–Crafts reaction (Table S1). Conversely, the variant LmrR_A92E_M8D, which gave the best results in the Friedel–Crafts reaction, did not give rise to improved activity and selectivity in the Diels–Alder reaction (Table S6). This shows that the active site of the LmrR-based ArM can be tailored specifically for catalysis of mechanistically different reactions. Understanding of the structural effect of these different mutations and their role in catalysis is not easily rationalized and will require molecular dynamics studies, as we performed before for the A92E mutation.[24]

Discussion

The remarkable and unexpected aspects of the current study are the straightforward in vivo assembly and apparent stability of the LmrR/Cu^{II}-Phen artificial metalloenzymes in the cell's cytoplasm, as evident from the catalysis data, inhibition studies, cell fractionation experiments and the in-cell NMR studies. *E. coli* cells over-expressing the protein LmrR are simply incubated with Cu^{II}-Phen abiological cofactor, resulting in uptake of the abiological cofactor and in vivo ArM assembly. For almost all ArM catalysis in vivo, the ArM and/or the bacterial cell had to be engineered to transport and localize the protein in the periplasm or on the cell surface, to reduce exposure to glutathione that is detrimental to many transition-metal complexes.[7,10,15]

Copper complexes are also expected to be readily reduced to Cu^{I} and then be toxic to the cell due to the formation of reactive oxygen species (ROS). Yet, the combined results demonstrate unequivocally that the assembled LmrR/Cu^{II} artificial metalloenzymes are stable and catalytically active in the cytoplasm of the cell. This was further verified by performing the Friedel–Crafts reaction with isolated LmrR_A92E_M8D/ Cu^{II}-Phen ArM in the presence of increasing amounts of glutathione, which is usually the main culprit for deactivation and instability of metal complexes and ArMs in cellular environments. The results indeed show that the ArM is still active in the presence of moderate concentrations of GSH (1 mM) and only at higher concentrations (10 mM) a significant detrimental effect on catalytic activity is observed, albeit that activity and enantioselectivity is even then still observed (Table S3). We hypothesize that the Cu^{II}-Phen complex bound to the front entrance of the binding pocket of LmrR is protected from GSH, and other cellular components. The front entrance where the Cu^{II} ion is located has an overall negative charge due to the presence of multiple carboxylate rich residues. This may cause charge repulsion with glutathione and in this way protect the metal complex, as was recently reported also for a glycosylated albumin artificial metalloenzyme.[45] Intriguingly, this is reminiscent of the biological role of the protein LmrR, which has evolved to rapidly bind a plethora of different toxic compounds entering the cell, as start of the cellular drug resistance response in Lactococcus lactis.[20,31]

Conclusion

In conclusion, we have demonstrated herein that catalytically active artificial metalloenzymes can be self-assembled in the cytoplasm of *E. coli* from heterologously produced LmrR and an exogenously added Cu^{II}-Phen complex. The unique aspect of our system is that no extensive engineering of the microbial host, the protein scaffold or the cofactor is required, which makes it attractive for applications in whole cell biocatalysis and directed evolution, as demonstrated here. Further evolution is envisioned to give rise to mutants with catalytic efficiencies that can become competitive with natural enzymes. Moreover, in view of the catalytic versatility of LmrR-based artificial metalloenzymes,[23,41] this work represents an important step forward towards achieving a hybrid metabolism by integrating artificial metalloenzymes in biosynthetic pathways.[6,16]

Acknowledgements

We thank L. Villarino for assistance with synthetic chemistry, Dr. A. Iyer for assistance with live cell confocal microscopy, R. Leveson-Gower for assistance with the MS measurements, Prof. P. Tordo, Dr. O. Ouari (Aix-Marseille Université) for providing AMUPol for the DNP experiments and Dr. C. Mayer for advice and discussions. We thank Prof. I. Shimada (U. of Tokyo) for the NMR assignments of the wild-type LmrR and Dr. H. van Ingen for providing access to the solution-state NMR instrument along with J. van der Zwan and Dr. S. Xiang for technical support and discussions. This work was supported by the Netherlands Organisation for Scientific Research (NWO, projects 700.26.121 and 700.10.443 to M.B. and 724.013.003 to G.R.). In addition, S.N. was supported by the Netherlands' Magnetic Resonance Research School (NMARRS, project number 022.005.029). G.R. acknowledges support from the Netherlands Ministry of Education, Culture and Science (Gravitation program no. 024.001.035).

Conflict of interest

The authors declare no conflict of interest.

Keywords: artificial metalloenzymes · biocatalysis · copper · in cell NMR spectroscopy · in vivo catalysis

[1] F. Schwizer, Y. Okamoto, T. Heinisch, Y. Gu, M. M. Pellizzoni, V. Lebrun, R. Reuter, V. Kohler, J. C. Lewis, T. R. Ward, *Chem. Rev.* **2018**, *118*, 142 – 231.
[2] M. Wilson, G. Whitesides, *J. Am. Chem. Soc.* **1978**, *100*, 306 – 307.
[3] T. K. Hyster, T. R. Ward, *Angew. Chem. Int. Ed.* **2016**, *55*, 7344 – 7357; *Angew. Chem.* **2016**, *128*, 7468 – 7482.
[4] U. Markel, D. F. Sauer, J. Schiffels, J. Okuda, U. Schwaneberg, *Angew. Chem. Int. Ed.* **2019**, *58*, 4454 – 4464; *Angew. Chem.* **2019**, *131*, 4500 – 4511.
[5] R. B. Leveson-Gower, C. Mayer, G. Roelfes, *Nat. Rev. Chem.* **2019**, *3*, 687 – 705.
[6] M. Jeschek, S. Panke, T. R. Ward, *Trends Biotechnol.* **2018**, *36*, 60 – 72.
[7] Y. M. Wilson, M. Duerrenberger, E. S. Nogueira, T. R. Ward, *J. Am. Chem. Soc.* **2014**, *136*, 8928 – 8932.
[8] M. Martínez-Calvo, J. L. Mascareñas, *Coord. Chem. Rev.* **2018**, *359*, 57 – 79.
[9] P. Destito, C. Vidal, F. Lopéz, J. L. Mascarenas, *Chem. Eur. J.* **2020**, https://doi.org/10.1002/chem.202003927.
[10] M. Jeschek, R. Reuter, T. Heinisch, C. Trindler, J. Klehr, S. Panke, T. R. Ward, *Nature* **2016**, *537*, 661 – 665.
[11] T. Heinisch, F. Schwizer, B. Garabedian, E. Csibra, M. Jeschek, J. Vallapurackal, V. B. Pinheiro, P. Marliere, S. Panke, T. R. Ward, *Chem. Sci.* **2018**, *9*, 5383 – 5388.
[12] A. R. Grimm, D. F. Sauer, T. Polen, L. Zhu, T. Hayashi, J. Okuda, U. Schwaneberg, *ACS Catal.* **2018**, *8*, 2611 – 2614.
[13] W. Ghattas, V. Dubosclard, A. Wick, A. Bendelac, R. Guillot, R. Ricoux, J. Mahy, *J. Am. Chem. Soc.* **2018**, *140*, 8756 – 8762.
[14] J. Zhao, J. G. Rebelein, H. Mallin, C. Trindler, M. M. Pellizzoni, T. R. Ward, *J. Am. Chem. Soc.* **2018**, *140*, 13171 – 13175.
[15] A. D. Liang, J. Serrano-Plana, R. L. Peterson, T. R. Ward, *Acc. Chem. Res.* **2019**, *52*, 585 – 595.
[16] J. Huang, Z. Liu, B. Bloomer, D. Clark, A. Mukhopadhyay, J. Keasling, J. Hartwig, *ChemRxiv* **2020**, https://doi.org/10.26434/chemrxiv.11955174.
[17] E. W. Reynolds, T. D. Schwochert, M. W. McHenry, J. W. Watters, E. M. Brustad, *ChemBioChem* **2017**, *18*, 2380 – 2384.
[18] M. Bordeaux, R. Singh, R. Fasan, *Bioorg. Med. Chem.* **2014**, *22*, 5697 – 5704.
[19] G. Sreenilayam, R. Fasan, *Chem. Commun.* **2015**, *51*, 1532 – 1534.
[20] H. Agustiandari, J. Lubelski, H. van Saparoea, B. van den Berg, O. P. Kuipers, A. J. M. Driessen, *J. Bacteriol.* **2008**, *190*, 759 – 763.
[21] P. K. Madoori, H. Agustiandari, A. J. M. Driessen, A. W. H. Thunnissen, *EMBO J.* **2009**, *28*, 156 – 166.
[22] J. Bos, W. R. Browne, A. J. M. Driessen, G. Roelfes, *J. Am. Chem. Soc.* **2015**, *137*, 9796 – 9799.
[23] G. Roelfes, *Acc. Chem. Res.* **2019**, *52*, 545 – 556.
[24] L. Villarino, S. Chordia, L. Alonso-Cotchico, E. Reddem, Z. Zhou, A. M. T. Thunnissen, J.-D. Maréchal, G. Roelfes, *ACS Catal.* **2020**, *10*, 11783 – 11790.
[25] E. van Bloois, R. T. Winter, D. B. Janssen, M. W. Fraaije, *Appl. Microbiol. Biotechnol.* **2009**, *83*, 679 – 687.
[26] M. Tabaka, L. Sun, T. Kalwarczyk, R. Holyst, *Soft Matter* **2013**, *9*, 4386 – 4389.
[27] Z. Serber, A. Keatinge-Clay, R. Ledwidge, A. Kelly, S. Miller, V. Dotsch, *J. Am. Chem. Soc.* **2001**, *123*, 2446 – 2447.
[28] S. Narasimhan, S. Scherpe, A. L. Paioni, J. van der Zwan, G. E. Folkers, H. Ovaa, M. Baldus, *Angew. Chem. Int. Ed.* **2019**, *58*, 12969 – 12973; *Angew. Chem.* **2019**, *131*, 13103 – 13107.
[29] S. Narasimhan, C. Pinto, A. L. Paioni, J. van der Zwan, G. E. Folkers, M. Baldus, *Nat. Protoc.* **2021**, https://doi.org/10.1038/s41596-020-00439-4.
[30] K. Takeuchi, Y. Tokunaga, M. Imai, H. Takahashi, I. Shimada, *Sci. Rep.* **2014**, *4*, 6922.
[31] J. P. van der Berg, P. K. Madoori, A. G. Komarudin, A. Thunnissen, A. J. M. Driessen, *PLoS One* **2015**, *10*, e0135467.
[32] K. Takeuchi, M. Imai, I. Shimada, *Sci. Rep.* **2017**, *7*, 267.
[33] F. Almeida, G. Amorim, V. Moreau, V. Sousa, A. Creazola, T. Americo, A. Pais, A. Leite, L. Netto, R. Giordano, A. Valente, *J. Magn. Reson.* **2001**, *148*, 142 – 146.
[34] L. Galvão-Botton, A. Katsuyama, C. Guzzo, F. Almeida, C. Farah, A. Valente, *FEBS Lett.* **2003**, *552*, 207 – 213.
[35] L. A. Baker, M. Daniels, E. A. W. van der Cruijsen, G. E. Folkers, M. Baldus, *J. Biomol. NMR* **2015**, *62*, 199 – 208.
[36] L. A. Baker, T. Sinnige, P. Schellenberger, J. de Keyzer, C. A. Siebert, A. J. M. Driessen, M. Baldus, K. Grunewald, *Structure* **2018**, *26*, 161 – 170.
[37] M. Kaplan, S. Narasimhan, C. de Heus, D. Mance, S. van Doorn, K. Houben, D. Popov-Čeleketić, R. Damman, E. A. Katrukha, P. Jain, W. J. C. Geerts, A. J. R. Heck, G. E. Folkers, L. C. Kapitein, S. Lemeer, P. M. P. van Bergen en Henegouwen, M. Baldus, *Cell* **2016**, *167*, 1241 – 1251.
[38] T. Viennet, A. Viegas, A. Kuepper, S. Arens, V. Gelev, O. Petrov, T. N. Grossmann, H. Heise, M. Etzkorn, *Angew. Chem. Int. Ed.* **2016**, *55*, 10746 – 10750; *Angew. Chem.* **2016**, *128*, 10904 – 10908.
[39] E. J. Koers, E. A. W. van der Cruijsen, M. Rosay, M. Weingarth, A. Prokofyev, C. Sauvee, O. Ouari, J. van der Zwan, O. Pongs, P. Tordo, W. E. Maas, M. Baldus, *J. Biomol. NMR* **2014**, *60*, 157 – 168.
[40] S. I. Volentini, R. N. Farias, L. Rodriguez-Montelongo, V. A. Rapisarda, *Biometals* **2011**, *24*, 827 – 835.
[41] L. Villarino, K. E. Splan, E. Reddem, L. Alonso-Cotchico, C. Guttierez de Souza, A. Lledos, J. Maréchal, A. W. H. Thunnissen, G. Roelfes, *Angew. Chem. Int. Ed.* **2018**, *57*, 7785 – 7789; *Angew. Chem.* **2018**, *130*, 7911 – 7915.
[42] Z. Zhou, G. Roelfes, *Nat. Catal.* **2020**, *3*, 289 – 294.
[43] S. Otto, F. Bertoncin, J. Engberts, *J. Am. Chem. Soc.* **1996**, *118*, 7702 – 7707.
[44] J. Bos, F. Fusetti, A. J. M. Driessen, G. Roelfes, *Angew. Chem. Int. Ed.* **2012**, *51*, 7472 – 7475; *Angew. Chem.* **2012**, *124*, 7590 – 7593.
[45] S. Eda, I. Nasibullin, K. Vong, N. Kudo, M. Yoshida, A. Kurbangalieva, K. Tanaka, *Nat. Catal.* **2019**, *2*, 780 – 792.

Manuscript received: November 4, 2020
Accepted manuscript online: January 11, 2021
Version of record online: February 1, 2021

